Comparative adsorption of ciprofloxacin on sugarcane bagasse from Ecuador and on commercial powdered activated carbon.

María E. Peñafiel[a]*, José M. Matesanz[b], Daniel Bermejo[a], Eulalia Vanegas[a], Rosa Mosteo[b], María P. Ormad[b]

[a] *Center for Environmental Studies. Department of Applied Chemistry and Production Systems, Faculty of Chemical Sciences, University of Cuenca, Cuenca, Ecuador.*

[b] *Water and Environmental Health Research Group, Environmental Sciences Institute (IUCA) Department of Chemical Engineering and Environmental Technology School of Engineering and Architecture (EINA), University of Zaragoza, Zaragoza, Spain.*

*María Eulalia Peñafiel, University of Cuenca, Av. 12 de Abril, 010203, Cuenca, Ecuador.
Corresponding Author: maria.penafiel@ucuenca.edu.ec. Telephone number 593991475901, ORCID 0000-0002-5807-5553

*Graphical Abstract

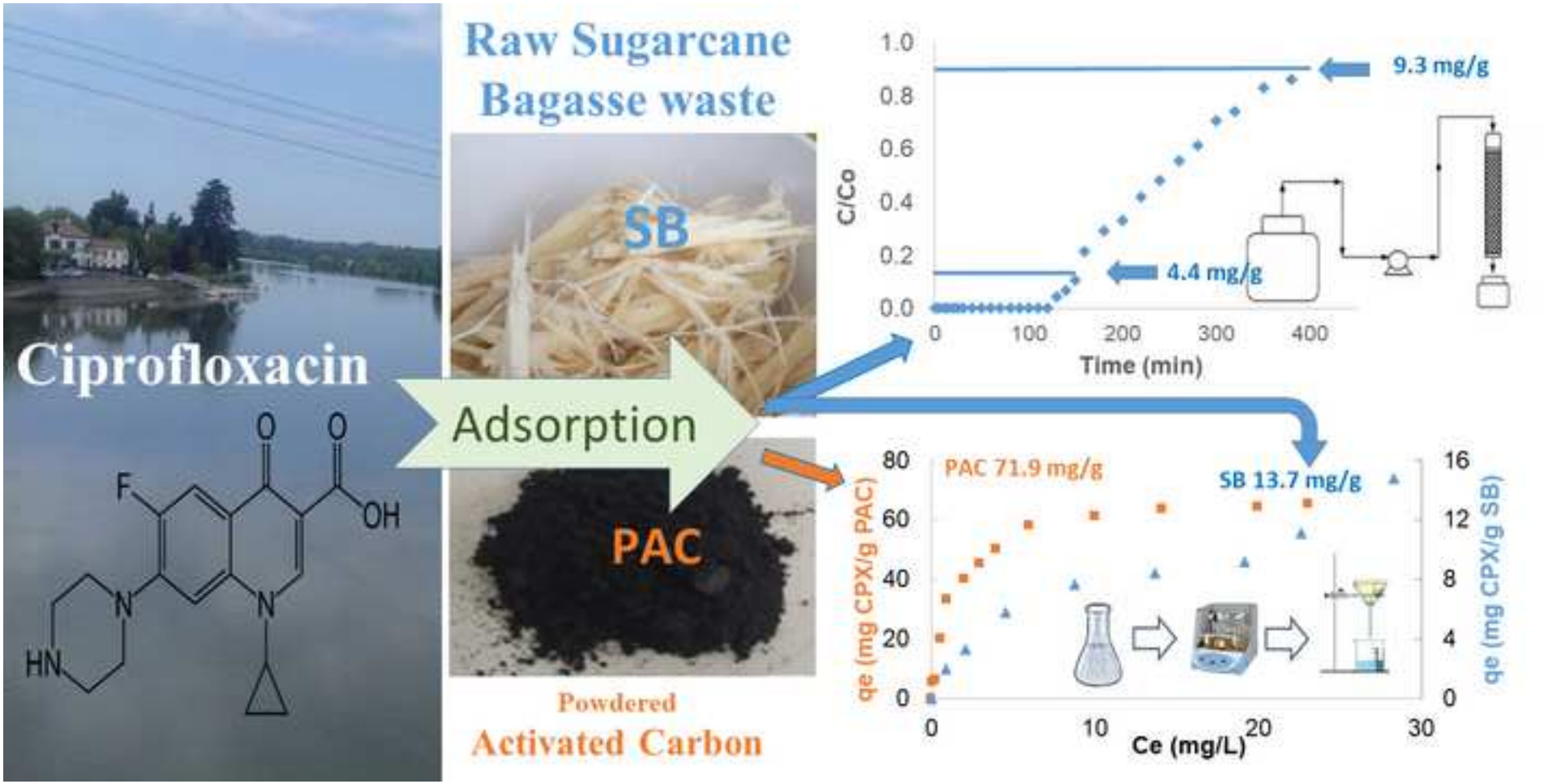

***Highlights (for review : 3 to 5 bullet points (maximum 85 characters including spaces per bullet point)**

- The uptake capacity (13.6 mg/g) shows sugarcane bagasse as a low-cost adsorbent.
- Activated carbon and bagasse removed up to 77% of ciprofloxacin from water.
- Bagasse adsorption fits BET, pseudo 2nd order and Bohart-Adams models.
- The bagasse kinetic shows a rapid physisorption controlled by external diffusion
- The adsorption capacity in fixed bed increases with a bed depth, reaching 4.4 mg/g

Comparative adsorption of ciprofloxacin on sugarcane bagasse from Ecuador and on commercial powdered activated carbon

María E. Peñafiel[a]*, José M. Matesanz[b], Eulalia Vanegas[a], Daniel Bermejo[a] Rosa Mosteo[b], María P. Ormad[b]

[a] *Center for Environmental Studies. Department of Applied Chemistry and Production Systems, Faculty of Chemical Sciences, University of Cuenca, Cuenca, Ecuador.*

[b] *Water and Environmental Health Research Group, Environmental Sciences Institute (IUCA) Department of Chemical Engineering and Environmental Technology School of Engineering and Architecture (EINA), University of Zaragoza, Zaragoza, Spain.*

*María Eulalia Peñafiel, University of Cuenca, Av. 12 de Abril, 010203, Cuenca, Ecuador.

Corresponding Author: maria.penafiel@ucuenca.edu.ec. Telephone number 593991475901, ORCID 0000-0002-5807-5553

ABSTRACT

This work examined the adsorption capacity of sugarcane bagasse (SB) for the removal of ciprofloxacin (CPX) from water using batch experiments and a fixed bed column and compared its adsorption performance with a powdered activated commercial carbon (PAC). Both adsorbents achieved a similar percentage removal of about 78 % with doses of 3 g L^{-1} of SB and 0.3 g L^{-1} of PAC (20 mg L^{-1} initial CPX concentration at 30°C). The maximum removal was obtained at a pH between 6 and 8. SB adsorption isotherms were fitted to the Langmuir, BET and Freundlich models showing a maximum adsorption capacity of 13.6 mg g^{-1}. The kinetic data for both SB and PAC fitted the pseudo second-order model (R^2=0.99). The adsorption process was faster on the SB (65% of elimination in the first 5 min) than on the PAC. The study of the adsorbent properties shows that SB is a macroporous solid with a specific surface area 250 times smaller than PAC. The thermodynamic results show that SB adsorption was physical and exothermic. The main suggested interactions between CPX and SB are electrostatic attraction, hydrogen bonding and dipole-dipole interactions. The experiments carried out in a fixed bed show that the adsorption capacity at breakthrough increases with the bed height. The adsorption capacity at saturation time was 9.47 mg g^{-1} at a flow rate of 3 mL min^{-1}, a bed height of 14 cm, and a diameter of 1.5 cm. The experimental data were fitted to

the Bohart-Adams model (R^2 = 0.98). These results highlight the capacity of sugarcane bagasse to adsorb ciprofloxacin from water, illustrating its potential as a low-cost adsorbent.

Keywords: Emerging contaminants, biowastes, equilibrium models, fixed bed column, low cost adsorption, valorization.

1. INTRODUCTION

The occurrence and persistence of pharmaceutical substances, especially antibiotics in surface waters, effluents from hospitals (1,2), and wastewater treatment plants (3–5) has led to the search for processes and techniques to remove drugs from aqueous solutions. Researches in recent years show that adsorption and degradation are the most extensively studied processes (6). In particular, efficient low-cost and environmentally friendly techniques are sought.

Recent studies have sought to use and develop various adsorbent materials with high specific surfaces and porous structures. These studies have shown the efficiency of many adsorbent materials such as graphene oxide (7–9), montmorillonite and kaolinite (10), carbon nanotubes (11,12), and activated carbon (13–16) for the removal of drugs from effluent waters. However, their preparation involves physical and chemical processes, which are expensive and can cause environmental problems. The main treatments used to obtain activated carbons are microwave assisted treatment, pyrolysis, and chemical treatment using H_3PO_4, $ZnCl_2$, KOH, NaOH, or H_2SO_4. Nanomaterials and active carbons are efficient but generally very expensive, which may limit their use on a real scale. Silva et al. (17) propose that the use of biowastes as adsorbents can be a win-win process because, in addition to giving economic value to waste, their management helps to protect the environment. In this work, the aim is the valorization of sugarcane bagasse produced in Ecuador as an adsorbent to remove ciprofloxacin from water.

Sugarcane bagasse (SB) is one of the biggest waste products in Ecuador and the world, representing approximately 30% of the weight of sugarcane production. The annual world production of sugarcane is approximately 1900 million tons and Ecuador produces approximately 8.6 million tons annually, as reported by the Food and Agriculture Organization of the United Nations. There are only a few

58 studies using raw sugarcane bagasse as an adsorbent. These include studies using bagasse for the
59 removal of contaminants such as dyes (4.6 mg dyes g^{-1} SB), heavy metals (28 Cr (III) mg g^{-1} SB), and
60 hydrocarbon (5 mL n-heptane g^{-1} SB) (18–20). There are no reports of studies using raw sugarcane
61 bagasse as an adsorbent to remove antibiotics from water.
62 Some research studies have proposed the use of raw residues as adsorbents. These studies have
63 shown the following differences between activated carbons and agricultural residues: (i) the value of
64 the specific surface of activated carbons varies from 400 to 1800 m^2 g^{-1} (21–23), while most organic
65 wastes have a very small specific surface area in the order of 1 to 13 m^2 g^{-1} (24–26); (ii) the chemical
66 composition and functional groups of the surface are different (27,28), and (iii) organic wastes are
67 generally macro-porous solids (24,29) while the active carbons are microporous (14). Despite these
68 differences, raw wastes can adsorb metals (30), dyes (31), and drugs (24). Therefore, other properties
69 such as the size and distribution of the pores, the chemistry of the surface, the size of the particles to
70 be adsorbed, the kinetic performance and the type of isotherm could influence the adsorption process.

71 Ciprofloxacin is one of the antibiotics commonly found in water (4,32,33). The primary route for
72 CPX to reach the aquatic environment is through the effluent from homes, hospitals, farms, and drug
73 manufacturers. The concentration of CPX (31 mg L^{-1}) in drug manufacturing effluent commonly
74 exceeds the toxic level for cyanobacteria and macrophytes (2). CPX has a high excretion rate;
75 approximately 50% of CPX is excreted by humans without metabolization (34).

76 In this work, a series of studies was carried out to evaluate the capacity, type and mechanism
77 adsorption of SB using batch experiments and fixed bed columns. The batch experiments were used to
78 analyze the influence of the dose of the adsorbents, the pH, the time of contact and the temperature.
79 Weber and Morris model, pseudo-first order and pseudo-second-order model were used to model the
80 kinetic data. Weber and Morris model also was used to describe the rate-controlling step. The
81 equilibrium data were fitted to different isotherm models (BET, Freundlich and Langmuir) to evaluate
82 the interaction of CPX with surface of adsorbent. The results were compared with the commercial
83 activated carbon adsorption process. Additionally, studies have been started to evaluate the possibility
84 of using bagasse in real purification processes, using fixed bed columns and scalable models such as

that of Bohart-Adams. Some properties such as the specific surface area, the pore distribution, the porosity, and the presence of functional groups on the adsorbent surface were examined to analyze the results and determine their role in the adsorption process.

2. MATERIALS AND METHODS

2.1 Adsorbate

Ciprofloxacin (with molecular weight 331.346 g mol^{-1}, size 0.825 nm, and pK_a values of 6.0 and 8.7) of analytical-reagent grade, from Sigma Aldrich, was used in this study. Because CPX is soluble in dilute hydrochloric acid, solutions were prepared with distilled water and 1% methanol at pH 3.5. The pH of the solutions was adjusted using HCl and NaOH, provided by Merck.

2.2 Sorbents

Sugarcane bagasse was collected in the Province of Azuay, Ecuador. The SB samples were washed three times with distilled water, dried in an oven at 60°C for 24 hours, and ground in a hammer mill. Particles between 0.4 and 0.8 mm were used. ChiemiVall supplied V-plus Commercial Powdered Activated Carbon (PAC), with a size less than 325 mesh, or 0.044 mm.

The adsorbent characteristics were determined by the adsorption/desorption of N_2, FESEM, FTIR, and elemental and immediate analysis using the methodology described in previous work (24). The zero load point (pH_{PZC}) was determined following the procedure used by Teixeira (26). The calorific power of the sorbents was determined using an isoperibolic PARR 6400 Calorimeter, applying the UNE-EN 14918 standard procedure.

2.3 Batch adsorption experiments

Batch adsorption experiments were carried out using the same methodology applied in previous works (24). The parameters examined were the dose of adsorbent (0.1 to 5 g L^{-1}), pH (2 to 10), contact time (2 to 180 min) and adsorption temperature (20, 30 and 40 °C). The experiments for the kinetic and equilibrium studies were carried out using doses of 0.3 g L^{-1} for PAC and 3 g L^{-1} for SB, and pH 6. The samples were filtered, and the final CPX concentrations were measured using a UV–VIS spectrophotometer (Shimadzu UV2550, Kyoto, Japan) at a wavelength of 272 nm.

The amount of CPX adsorbed per gram of adsorbent, also called the equilibrium adsorption capacity (q_e, mg g^{-1}) and the percentage of removal (% Removal) were calculated with the following equations.

$$q_e = \frac{(C_o - C_e)\,V}{m} \quad (1)$$

$$\%\ Removal = \frac{(C_o - C_e)\,100}{C_o} \quad (2)$$

where C_o and C_e are the initial and equilibrium concentration of CPX in the aqueous phase after adsorption (mg L^{-1}); V is the volume of the solution (L); and m is the mass of the adsorbent (g).

The adsorptive capacity was evaluated in a batch adsorption system, using the equilibrium and kinetic linearized forms of the adsorption models listed in Table 1.

To understand the adsorption mechanism, the thermodynamic parameters were evaluated. These parameters of CPX adsorption with SB and PAC were calculated by

$$\ln K_e = \frac{\Delta S^o}{R_g} - \frac{\Delta H^o}{R_g\,T} \quad (3)$$

$$\Delta G^0 = \Delta H^0 - T\,\Delta S^0 \quad (4)$$

$$K_e = \frac{1000\,K_L\ (molecular\ weight\ of\ adsorbate)[Adsorbate]^0}{\gamma} \quad (5)$$

where ΔG^o, ΔH^o, ΔS^o are the free energy, the enthalpy of adsorption, and the entropy of adsorption, respectively (KJ mol^{-1}); K_e is the thermodynamic equilibrium constant (dimensionless); T is the solution temperature (K); R_g is the gas constant (8.314 J mol^{-1} K^{-1}); K_L is the Langmuir constant (L mg^{-1}); 331.34 g mol^{-1} is the molar mass of CPX; $[Adsorbate]^0$ is the standard concentration of the adsorbate (1 mol L^{-1}) (41); and γ is the coefficient of activity (dimensionless) which is almost 1.0 in very dilute solutions.

2.4 Fixed bed experiments

The purpose of a fixed bed is to improve the contact between the adsorbent and adsorbate. This is currently the most common form of contact in the adsorption process (42). The experiments were performed using a column with an internal diameter of 1.5 cm and filled with different amounts of SB to obtain different bed heights: 4, 6, 8, 10 and 12 cm. All experiments were carried out with a constant downward flow rate of 3 mL min^{-1} (1.70 cm min^{-1}), a bed density of 0.142 g cm^{-3}, and an initial solution concentration of 10 mg L^{-1} (43). The permissible concentration of the effluent solution was

10% of the concentration at the inlet, that is, 1 mg L^{-1}. The time to reach this concentration was determined as the breakthrough time (t_b).

For the analysis of the adsorption process in fixed bed columns, we used the method based on the construction of effluent-time concentration curves, which is mainly based on the operating conditions, the equilibrium results and the surface characteristics (44).

The amount of CPX adsorbed at the breakthrough time (q_b) and saturation time (q_s) was calculated using the following equations (45).

$$q_s = \frac{C_0\, Q}{1000\ m}\int_0^{t_s}\left(1 - \frac{C_s}{C_0}\right) \qquad (6)$$

$$q_b = \frac{C_0\, Q}{1000\ m}\int_0^{t_b}\left(1 - \frac{C_b}{C_0}\right) \qquad (7)$$

where C_o, C_b and C_s are the initial solution concentration and the effluent concentration at the breakthrough time and the saturation time, respectively (mg L^{-1}); q_b and q_s are the adsorption capacity (mg g^{-1}) at the breakthrough and the saturation time; Q is the volumetric flow (mL min^{-1}); and t_b and t_s are the breakthrough and saturation time when C/C_o is respectively 0.1 and 0.9.

The results obtained were fitted with the Bohart-Adams model. This is an easy model that offers a simple and quick evaluation of the adsorption performance.

$$\ln\left(\frac{C_o}{C_t} - 1\right) = \frac{K_{BA}N_oH}{u} - K_{BA}C_o t \qquad (8)$$

where K_{BA} (L min^{-1} mg^{-1}) is the rate constant of the Bohart-Adams equation; N_o the maximum adsorptive capacity (mg L^{-1}); H the bed depth (cm); t the service time of the column (min); u the linear flow velocity (cm min^{-1}); and Ct the concentration at time t.

The percentage of fractional bed utilization (%FBU) can, according to Jaira et al. (45), be calculated as:

$$\%FBU = \left(\frac{q_b}{q_s}\right)100 \qquad (9)$$

$$MTZ = \left(1 - \frac{q_b}{q_s}\right) L \qquad (10)$$

where MTZ is the mass transfer zone (cm).

To normalize the results of the volume of influent treated in column, the concept of specific volume of water treated (BV) was used (46):

164 $$BV = \frac{V_b}{V_c} \quad (11)$$

165 where V_b is volume of influent treated (mL), V_c is volume of bed (mL) (V_c is calculated by column
166 area per bed height).

167 To compare adsorbents with different porosities, Mazur et al. (47) propose a modification of BV by
168 BV*: change volume of bed by volume of adsorbent used (Vr)

169 $$BV^* = \frac{V_b}{V_r} = \frac{V_b}{V_c\,(1-\xi)} \quad (12)$$

170 where: ξ = porosity

171 The determination coefficient (R^2) was used to evaluate the goodness of fit of the applied adsorption
172 models. All the experiments were done in triplicate.

173

174 **3. RESULTS AND DISCUSSION**

175 **3.1 Characterization of the adsorbents**

176 Figure 1 depicts the plots of the N_2 physisorption isotherm for sugarcane bagasse and PAC. SB
177 (Figure 1a) presents a type II isotherm with a rapid increase in high pressure adsorption and a type H-
178 3 hysteresis loop that closes after the relative pressure of 0.4, indicating the formation of a multilayer
179 and the presence of macroporosity (24). The isothermal form of PAC corresponds to type I and has an
180 H-4 type hysteresis loop similar to most microporous activated carbons. In the relatively small non-
181 microporous portion of SB, the H-3 loop is equivalent to an H-4 loop (48).

182 Table 2 presents the physical parameters of both adsorbents. PAC shows a high surface area of 643.97
183 $m^2\ g^{-1}$, while SB has a considerably lower value, 2.55 $m^2\ g^{-1}$, which is greater than the 0.487 $m^2\ g^{-1}$
184 found by Moubarik et al. (49). The values of S_{BET} and pore volume of PAC are similar to the values
185 found in other studies (50,51). These results would indicate a clear disadvantage of SB compared to
186 PAC as an adsorbent.

187 As illustrated in Figure 2, PAC shows a uniform pore distribution with a diameter less than 0.6 nm,
188 while the pore size distribution of SB is more dispersed with predominant larger pores. The total pore
189 volume of SB is 0.0065 $cm^3\ g^{-1}$, while that of PAC has 0.3569 $cm^3\ g^{-1}$ of total pore volume of which
190 0.2847 $cm^3\ g^{-1}$ is volume of micropores.

Figure 3 shows that the surface of PAC is microporous, while the surface of the SB shows large cavities like to that of the corncobs used in previous work. (24).

The chemical properties and the caloric power of both sorbents are listed in Table 3. According to the ultimate and proximate analysis, the difference between PAC and SB is the amount of carbon and oxygen. The PAC has a greater amount of carbon, while the SB has more oxygen (52) .The pH_{PZC} of SB is 5.9, similar to the findings of other studies (18,49), while PAC has an almost neutral pH_{PZC} with a value of 7.6.

The spectra of the FTIR analysis for SB and PAC are depicted in Figure 4. Functional groups and their wavenumbers for both adsorbents are listed in Table 4. The large number of functional groups in SB is due to its high oxygen and hydrogen content.

3.2 Batch adsorption studies

Adsorbent dosage

In order to find the dose of adsorbent at which the maximum percentage of adsorbed CPX is achieved, an initial CPX solution of 20 mg L^{-1} at pH 6 was shaken for 120 min at 150 rpm with different amounts of each adsorbent. The removal efficiency increased as the adsorbent dose increased. As can be deduced from Figure 5, a dose of 3 g SB L^{-1} and 0.3 g PAC L^{-1} yield the same CPX removal percentage, approximately 78%. Even though the PAC has a specific surface area 250 times smaller than PAC, both adsorbents achieve the same elimination percentage with a dose of SB 10 times greater than PAC, which indicates that the surface area is likely not the only responsible factor in the adsorption process (12). These results indicate a high adsorption capacity per surface for SB (2.24 mg m^{-2}) compared to PAC (0.077 mg m^{-2}) (59). Given that an increase in these doses for both adsorbents did not show a significant improvement in the removal percentage, it was decided to use these doses in the subsequent studies.

Effect of pH

The effect of the pH on the removal percentage using a CPX solution of 20 mg L^{-1} was investigated. The results are shown in Figure 6. The speciation of the drug plays an important role in the adsorption process. CPX is a zwitterionic drug. At pH between 5.9 and 8.0 it is in its zwitterionic form

possessing simultaneously a region with a positive charge and another region with a negative charge (60). CPX is cationic for pH-values below 5.9 and anionic for pH-values above 8.0.

Both adsorbents reached the removal percentage of 78% at a pH between 6 and 8, just in the zwitterionic zone of the CPX. The value of pH 6 was taken as optimal for this study. At pH below 6, a significant decrease in adsorption efficiency was observed, because SB (pH_{PZC} = 5.9), PAC (pH_{PZC} = 7.6) and CPX have a positive charge, which favors electrostatic repulsion, this being more significant for the SB. Furthermore, CPX is more soluble in an acidic solution, which makes adsorption difficult. Increasing the pH above 8 reduces the adsorption of CPX. When the pH>8 the adsorbents and drug are anionic, so they can be electrostatically repellent. The adsorption of CPX is maximum when the form of the hybrid ion and the adsorbents have zero charges, perhaps because there is no electrostatic repulsion, and CPX can interact with the deprotonated and protonated functional groups of the adsorbent. The formation of hydrogen bonds and dipole attractions, especially by fluorine of CPX (61), would aid in the adsorption of CPX.

Sorption kinetics

The kinetic adsorption performance of CPX on SB and PAC was examined at different times to study the speed of adsorption, the time required to reach equilibrium and the adsorption mechanism. As shown in Figure 7, the equilibrium is reached in 60 min for SB and 100 min for PAC, achieving the CPX removal percentage of 78%. A rapid adsorption is observed on SB while the adsorption process on the PAC is slower. Many studies show similar equilibrium times of CPX adsorption on activated carbons (53,60,62).

Three kinetic models were used to understand the behavior of the adsorbents and examine the kinetic controlling mechanism. The kinetic data were examined by the pseudo-first order, pseudo-second order, and Weber and Morris models. The parameters of the kinetic equations, as well as the correlation coefficient of the experimental data, are presented in Table 5. The correlation coefficients (R^2=0.99) indicate that the adsorption follows a second order kinetic model for the two adsorbents. The linearized pseudo-second order plot is shown in Figure 8; the pseudo-first order plot is shown in the supplementary material (Figure S2). These results, as suggested by Chen and co-workers (8), indicate that sorption for both adsorbents is controlled by multiple processes: chemisorption and

247 physisorption (29). There is no clear line between the two adsorption mechanisms (63). The kinetic
248 constant K_2 for SB (0.09 g mg^{-1} min^{-1}) is higher than for PAC (0.0045 g mg^{-1} min^{-1}), also indicating
249 that adsorption on SB is more rapid (24).
250 The Weber and Morris intraparticle diffusion model highlighted the difference between the SB and
251 PAC adsorption mechanisms. In both cases, intraparticle diffusion is not the only rate-controlling step
252 in the process (24). PAC has three linear portions (Figure 9), which implies that the adsorption of
253 CPX in PAC goes through three successive stages until equilibrium: 1) external diffusion, 2)
254 intraparticle diffusion, and 3) sorption (64,65). SB exhibits only one adsorption process, external
255 diffusion (24), which would justify the higher rate of adsorption on the Sb. For PAC, the third stage
256 (the adsorption stage) was fast, indicating that the mass transfer process would be controlled by
257 external and internal diffusion. As shown in Figure 9 and the results presented in Figure 7, PAC
258 adsorbs almost 45% of the CPX in 20 min in the external diffusion stage (the first linear segment) and
259 reaches 70% in the intraparticle diffusion process, while SB adsorbs 65% of the CPX in the first 5
260 min. The value of the boundary layer thickness for the PAC is C = 27.31 mg g^{-1}, greater than the value
261 of C = 2.87 mg g^{-1} for the SB, indicating that PAC has a much thicker initial layer. Notwithstanding
262 the difference, both values represent approximately 50% of the total adsorption capacity.
263 The R_i (the initial adsorption factor) values for PAC and SB are 0.51 and 0.18 mg g^{-1} $min^{-1/2}$
264 respectively, indicating intermediate initial adsorption ($0.9>R_i>0.5$) for PAC and strong initial
265 adsorption ($0.5>R_i>0.1$) for SB. The result for the SB is important because according to Wu et al (40),
266 only 1 in every 3 adsorbents have similar R_i values.
267 The adsorption capacity of CPX on PAC is less than that achieved by activated carbons in other
268 studies (9). In a type I isotherm, the adsorption limit is governed by the accessible micropores (66). In
269 this study, the molecular length of CPX was 0.825 nm (67), and it could not access the majority of the
270 pores of the PAC (0.6 nm in size), confirming that the adsorption capacity depends on the size of the
271 pores. The micropores of PAC, in this case, reduces the adsorption of CPX. The cavities and large
272 pores of SB allow easy access for the CPX particles, and these can better interact with the surface of
273 SB (12).
274 ***Equilibrium studies***

The equilibrium study was performed with doses of 3.0 and 0.3 g L^{-1} for SB and PAC, respectively, equilibration times of 100 min for PAC and 60 min for SB, and temperatures of 20, 30, and 40°C.

In both adsorbents, an increase in adsorption capacity was observed with increased CPX concentration, but a higher removal percentage was achieved at the lower initial concentration. The parameters and the coefficient of correlation (R^2) of the Langmuir, Freundlich and BET models are listed in Table 6. The experimental data of PAC better fitted the Langmuir model, with an R^2 value of 0.99. The behavior of the PAC adsorption process is similar to that found in other investigations using active carbons or microporous materials (8,56,62).

As illustrated in Figure 10, the adsorption of CPX on SB is adjusted to a type II isotherm, as seen in the N_2 adsorption depicted in Figure 1. The main characteristic of a type II isotherm is the formation of multilayers. The nature of the forces that make up the multiple layers is physical (63). The SB experimental data fit well to the BET and Freundlich models. According to the BET model, in multilayer formation, once a molecule is adsorbed it acts as an active site in which other molecules can be adsorbed (37).

As indicated by the Langmuir model, the maximum adsorption capacity is 13.7 and 71.9 mg g^{-1} for SB and PAC, respectively. The values of R_L (separation factor) indicate favorable adsorption for the two adsorbents ($0<R_L<1$). The values of the exponent n (adsorption intensity) in the Freundlich model are greater than 1, which also indicates a favorable adsorption process.

SB showed a greater adsorption capacity of CPX than sodium alginate hydrogel (8.66 mg g^{-1}) (7), modified coal fly ash (1.44 mg g^{-1}) (68) and schorl (5.6 mg g^{-1}) (54); a similar capacity to calcium alginate (15.57 mg g^{-1}) (9); and a smaller capacity than bamboo-based activated carbon (108 mg g^{-1}) (14) and enteromorpha prolifera (21.7 mg g^{-1}) (69).

Effect of temperature

As can be seen in Figure 11, increasing the temperature lowers the percentage of CPX adsorbed on SB and increases the CPX adsorbed of PAC.

The thermodynamic parameters ($\Delta G°$, $\Delta H°$, $\Delta S°$) are listed in Table 7. The negative value of $\Delta G°$ indicates the process is favorable and spontaneous for both adsorbents. The negative $\Delta H°$ values for

SB suggest an exothermic process, while a positive ΔH° value for PAC shows an endothermic process.

The increase in absolute values of ΔG° (-23.14, -24.84 and -27.51 kJ mol^{-1}) with increasing temperature shows a greater capacity for adsorption of CPX at high temperatures in PAC (27), while the ΔG° values for SB show a small decrease (-26.99, -26.83 and -26.56 kJ mol^{-1}). The boundaries between fission and chemisorption are variable. Some authors suggest that the adsorption enthalpy for physisorption is lower than 40 kJ/mol^{-1} (21,29) while others state that the value of ΔH° would be less than 50 kJ mol^{-1} (70). In any case, the adsorption of CPX on SB is physical in nature (28.35 kJ mol^{-1}), the main suggested interactions between CPX and SB being electrostatic, hydrogen bonding, and dipole-dipole interactions. The ΔH° value for CPX adsorption on PAC was slightly above the limit for physisorption (40 kJ mol^{-1}), suggesting that the process can be simultaneously physisorption and chemisorption. The positive ΔS° values suggest the affinity of the sorbents with the adsorbents (71).

3.3 Fixed bed adsorption studies

The objective of fixed bed adsorption studies is to determine the effect of the bed height on the breakthrough curve. Fixed bed experiments were carried out at a downward flow rate of 3 ml min^{-1}, a constant bed density of 0.142 g cm^{-3}, and an initial CPX concentration of 10 mg L^{-1}. The breakthrough curves at different bed depths are shown in Figure 12 (4, 6, 8, 10, 12, and 14 cm), and the main results summarized in Table 8. Increasing the bed height increases the service adsorption capacity at breakthrough time (q_b), and the total amount of CPX adsorbed at saturation time. As the bed depth increases, the fractional bed utilization (FBU) also increases. The volume treated by increasing the bed depth bed from 4 to 14 cm goes from 66 (9.4 BV, 19.5 BV*) to 435 (17.6 BV, 36.8 BV*) mL, and the adsorption capacity from 2.05 to 4.4 mg g^{-1} (72). Conversely, when the bed height increases, the adsorption capacity at saturation time (q_s) decreases. A lower bed height shows faster bed exhaustion (72). Although the MTZ value increases, the adsorption capacity also increases because the ratio of the bed height to the MTZ decreases from 82% (4 cm) to 52% (14 cm) (47).

The relationship between the bed depth and the service time at different effluent concentrations is shown in Figure 13. In all cases, the experimental data fitted a straight line. This adjustment presents

similar slopes up to C_s/C_o = 0.5, increasing slightly for C_s/C_o = 0.9. This increase in service time close to saturation was due to the increase of % FBU.

A value of H/d>5 is recommended for the scaling up of experimental data from a small to a large scale (42), with the objective of avoiding the maldistribution of liquid in larger beds. In this study, beds with heights greater than 8 cm meet the H/d ratio.

Table 9 shows the results obtained by applying the Bohart-Adams model to the experimental data of the initial part of the adsorption process (C_t/C_o<0.5). The parameters of the Bohart-Adams model were estimated applying linear regression on the plots of $ln\left(\frac{C_o}{C_t}-1\right)$ versus time (Supplementary material, Figure S3). This table shows the decrease of the mass transfer coefficient with the increasing depth of the bed, similar to findings reported by Nazari et al. (73) using a walnut shell-based activated carbon, which indicates that the process is dominated by external mass transfer (74).

4. CONCLUSIONS

The present study demonstrated that sugar bagasse can adsorb ciprofloxacin (CPX) in water, presenting good results both in the percentage of elimination and in the time necessary for the elimination. Some of these results were compared with adsorption of CPX on a powdered activated carbon (PAC).

The SB has a S_{BET} of 2.55 $m^2\ g^{-1}$ compared to 644 $m^2\ g^{-1}$ for PAC; in addition, these substances differ in that micropores predominate in the PAC while mesopores predominate in the SB.

At an initial concentration of 20 mg CPX L^{-1}, and doses of 3 g SB L^{-1} and 0.3 g PAC L^{-1}, a CPX elimination percentage of 78% is achieved for both adsorbents, and an adsorption capacity of 5.7 mg CPX g^{-1} for SB and 50.1 mg CPX g^{-1} for PAC. The maximum elimination of CPX is achieved at a pH between 6 and 8. The saturation time is reached at 60 min for SB (65% of elimination in the first 5 min) and 100 min for PAC. As the temperature increases, the adsorption capacity of PAC increases, while that of bagasse decreases.

Column tests of 1.5 cm in diameter were performed, with a bed density of 0.142 g cm^{-3}, a downward flow rate of 3 mL min^{-1} and different bed heights. Increasing the length of the bed increases the

volume of the treated effluent and the adsorption capacity. For a C_s/C_o<0.1, the time of service and treated volume varies from 22 min and 66 ml in the 4 cm column to 145 min and 435 ml in the 14 cm column respectively, and the adsorption capacity ranges from 2.5 to 4 mg g^{-1}. The percentage of the fractional bed utilization (%FBU) increases with the height of the column, being 17% for a bed height of 4 cm, and up to 41% for a 14 cm bed height. The experimental data fitted well to the Bohart-Adams model.

Acknowledgements

The authors would like to acknowledge the use of the Servicio General de Apoyo a la Investigación-SAI, Universidad de Zaragoza, and the Dirección de Investigación de la Universidad de Cuenca (DIUC) through the project DUIC_XIV_2016_037. Special thanks to Dr. Jan Feyen.

References

1. Li, C., Lu, J., Liu, J., Zhang, G., Tong, Y., & Ma, N. Exploring the correlations between antibiotics and antibiotic resistance genes in the wastewater treatment plants of hospitals in Xinjiang, China. *Environmental Science and Pollution Research*. 2016; *23*(15), 15111-15121.

2. Larsson, D. J., de Pedro, C., & Paxeus, N. Effluent from drug manufactures contains extremely high levels of pharmaceuticals. *Journal of hazardous materials*. 2007; *148*(3), 751-755.

3. Hamza RA, Iorhemen OT, Tay JH. Occurrence, impacts and removal of emerging substances of concern from wastewater. Environmental Technology & Innovation. 2016; 5:161–175.

4. Guerra P, Kim M, Shah A, Alaee M, Smyth SA. Occurrence and fate of antibiotic, analgesic / anti-in fl ammatory , and antifungal compounds in fi ve wastewater treatment processes. Science of the Total Environment. 2014;473-474:235–243

5. Luo Y, Guo W, Ngo HH, Nghiem LD, Hai FI, Zhang J, et al. A review on the occurrence of micropollutants in the aquatic environment and their fate and removal during wastewater treatment. Science of the Total Environment. 2014;473-474:619–641.

6. Akhtar, J., Amin, N. A. S., & Shahzad, K. A review on removal of pharmaceuticals from water by adsorption. *Desalination and Water Treatment*. 2016;*57*(27), 12842-12860

7. Fei, Y., Li, Y., Han, S., & Ma, J. Adsorptive removal of ciprofloxacin by sodium alginate/graphene oxide composite beads from aqueous solution. Journal of Colloid and Interface Science. 2016; 484, 196-204

8. Chen H, Gao B, Li H. Removal of sulfamethoxazole and ciprofloxacin from aqueous solutions by graphene oxide. Journal of Hazardous Materials. 2015;282:201–207

9. Wu S, Zhao X, Li Y, Zhao C, Du Q, Sun J, et al. Adsorption of ciprofloxacin onto biocomposite fibers of graphene oxide/calcium alginate. Chemical Engineering Journal. 2013;230:389–395

10. Pei, Z., Shan, X. Q., Kong, J., Wen, B., & Owens, G. Coadsorption of ciprofloxacin and Cu (II) on montmorillonite and kaolinite as affected by solution pH. *Environmental science & technology*. 2010; *44*(3), 915-920

11. Li, H., Zhang, D., Han, X., & Xing, B. Adsorption of antibiotic ciprofloxacin on carbon nanotubes: pH dependence and thermodynamics. *Chemosphere*. 2014; *95*, 150-155.

12. Carabineiro, S. A. C., Thavorn-Amornsri, T., Pereira, M. F. R., Serp, P., & Figueiredo, J. L. Comparison between activated carbon, carbon xerogel and carbon nanotubes for the adsorption of the antibiotic ciprofloxacin. *Catalysis Today*. 2012; *186*(1), 29-34.

13. Peng, X., Hu, F., Lam, F. L., Wang, Y., Liu, Z., & Dai, H. Adsorption behavior and mechanisms of ciprofloxacin from aqueous solution by ordered mesoporous carbon and bamboo-based carbon. *Journal of colloid and interface science*. 2015; *460*, 349-360

14. Wang, Y. X., Ngo, H. H., & Guo, W. S. Preparation of a specific bamboo based activated carbon and its application for ciprofloxacin removal. *Science of the Total Environment*. 2015; *533*, 32-39

15. Darweesh, T. M., & Ahmed, M. J. Adsorption of ciprofloxacin and norfloxacin from aqueous solution onto granular activated carbon in fixed bed column. *Ecotoxicology and environmental safety*. 2017; *138*, 139-145.

16. Gupta A, Garg A. Adsorption and oxidation of ciprofloxacin in a fixed bed column using activated sludge derived activated carbon. Journal of Environmental Management. 2019; 250 (December 2018).

17. Silva, C. P., Jaria, G., Otero, M., Esteves, V. I., & Calisto, V. Waste-based alternative adsorbents for the remediation of pharmaceutical contaminated waters: Has a step forward already been taken? Bioresource technology. 2018; *250*, 888-901.

18. Pathrbe MD, Dubey RS, Lataye DH, Maharashtra N. Removal of direct red 28 dye from aqueous solutions by using sugarcane bagasse as an adsorbent. 49th Annual Convention of IWWA on "Smart Water Management". 2017; 28: 1–9.

19. Ullah, I., Nadeem, R., Iqbal, M., & Manzoor, Q. Biosorption of chromium onto native and immobilized sugarcane bagasse waste biomass. *Ecological engineering*. 2013; *60*, 99-107.

20. Brandão PC, Souza TC, Ferreira CA, Hori CE, Romanielo LL. Removal of petroleum hydrocarbons from aqueous solution using sugarcane bagasse as adsorbent. Journal of Hazardous Materials. 2010; 175(1–3), 1106–1112

21. Tonucci, M. C., Gurgel, L. V. A., & de Aquino, S. F. Activated carbons from agricultural byproducts (pine tree and coconut shell), coal, and carbon nanotubes as adsorbents for removal of sulfamethoxazole from spiked aqueous solutions: Kinetic and thermodynamic studies. *Industrial crops and products* 2015; *74*, 111-121.

22. Martins AC, Pezoti O, Cazetta AL, Bedin KC, Yamazaki DAS, Bandoch GFG, et al. Removal of tetracycline by NaOH-activated carbon produced from macadamia nut shells: Kinetic and equilibrium studies. Chemical Engineering Journal. 2015;260, 291-299

23. Choi, K. J., Kim, S. G., Kim, C. W., & Kim, S. H. Effects of activated carbon types and service life on removal of endocrine disrupting chemicals: amitrol, nonylphenol, and bisphenol-A. *Chemosphere*. 2005; *58*(11), 1535-1545.

24. Peñafiel, M. E., Matesanz, J. M., Vanegas, E., Bermejo, D., & Ormad, M. P. Corncobs as a potentially low-cost biosorbent for sulfamethoxazole removal from aqueous solution. Separation Science and Technology. 2019; 1-12

25. Peng, S. H., Wang, R., Yang, L. Z., He, L., He, X., & Liu, X. Biosorption of copper, zinc, cadmium and chromium ions from aqueous solution by natural foxtail millet shell. Ecotoxicology and Environmental Safety. 2018; 165, 61-69..

26. Teixeira, S., Delerue-Matos, C., & Santos, L. Removal of sulfamethoxazole from solution by raw and chemically treated walnut shells. Environmental Science and Pollution Research. 2012; 19(8), 3096-3106.

27. Lin, H., Xu, J., Dong, Y., Wang, L., Xu, W., & Zhou, Y. Adsorption of heavy metal cadmium (II) ions using chemically modified corncob: mechanism, kinetics, and thermodynamics. *Desalination and Water Treatment*. 2016; *57*(39),18537-18550.

28. Reffas A, Bernardet V, David B, Reinert L, Lehocine MB, Dubois M, et al. Carbons prepared from coffee grounds by H3PO4 activation: Characterization and adsorption of methylene blue and Nylosan Red N-2RBL. Journal of Hazardous Materials. 2010;175(1-3):779–788

29. Antunes M, Esteves VI, Guégan R, Crespo JS, Fernandes AN, Giovanela M. Removal of diclofenac sodium from aqueous solution by Isabel grape bagasse. Chemical Engineering Journal. 2012;192:114–121

30. Calero, M., Ronda, A., Pérez, A., Yáñez, A., Trujillo, M. C., & Martín-Lara, M. Á. The scale-up of Cr3+ biosorption onto olive stone in a fixed bed column. *Desalination and Water Treatment*. 2016; *57*(52), 25140-25152

31. do Nascimento, G. E., Campos, N. F., da Silva, J. J., Barbosa, C. M. B. D. M., & Duarte, M. M. M. B. Adsorption of anionic dyes from an aqueous solution by banana peel and green coconut mesocarp. *Desalination and Water Treatment*. 2016; *57*(30), 14093-14108.

32. Gracia-Lor E, Sancho JV, Serrano R, Hernández F. Occurrence and removal of pharmaceuticals in wastewater treatment plants at the Spanish Mediterranean area of Valencia. Chemosphere. 2012;87(5):453–462.

33. Wilkinson, J., Hooda, P. S., Barker, J., Barton, S., & Swinden, J. Occurrence, fate and transformation of emerging contaminants in water: An overarching review of the field. *Environmental Pollution*. 2017; *231*, 954-970

34. Patrolecco L, Rauseo J, Ademollo N, Grenni P, Cardoni M, Levantesi C, et al. Persistence of the antibiotic sulfamethoxazole in river water alone or in the co-presence of ciprofloxacin. Science of the Total Environment. 2018;640:1438–1446

35. Foo, K. Y., & Hameed, B. H. Insights into the modeling of adsorption isotherm systems. Chemical Engineering Journal. 2010; 156(1), 2-10

36. Xiao, H., Peng, H., Deng, S., Yang, X., Zhang, Y., & Li, Y. Preparation of activated carbon from edible fungi residue by microwave assisted K2CO3 activation—application in reactive black 5 adsorption from aqueous solution. Bioresource Technology. 2012; 111, 127-133.

37. Ebadi A, Soltan Mohammadzadeh JS, Khudiev A. What is the correct form of BET isotherm for modeling liquid phase adsorption? Adsorption. 2009;15(1):65–73

38. Yuh-Shan, H. Citation review of Lagergren kinetic rate equation on adsorption reactions. Scientometrics. 2004; 59(1), 171-177.

39. Ho, Y. S., & McKay, G. Pseudo-second order model for sorption processes. Process Biochemistry. 1999; 34(5), 451-465

40. Wu, F. C., Tseng, R. L., & Juang, R. S. Initial behavior of intraparticle diffusion model used in the description of adsorption kinetics. Chemical Engineering Journal. 2009; 153(1-3), 1-8.

41. Lima EC, Hosseini-bandegharaei A, Moreno-piraján JC, Anastopoulos I. A critical review of the estimation of the thermodynamic parameters on adsorption equilibria . Wrong use of equilibrium constant in the Van ' t Hoof equation for calculation of thermodynamic parameters of adsorption. Journal of Molecular Liquids. 2019;273:425–434.

42. Inglezakis, V. J., & Poulopoulos, S. G. Adsorption, ion exchange and catalysis. 2006; (Vol. 3, pp. 498-520). Amsterdam: Elsevier.

43. Oliveira, M. F., de Souza, V. M., da Silva, M. G., & Vieira, M. G. Fixed-bed adsorption of caffeine onto thermally modified Verde-lodo bentonite. Industrial & Engineering Chemistry Research. 2018; 57(51), 17480-1748.

44. Noll, K. E. Adsorption technology for air and water pollution control. CRC Press. 1991.

45. Jaria, G., Calisto, V., Silva, C. P., Gil, M. V., Otero, M., & Esteves, V. I. Fixed-bed performance of a waste-derived granular activated carbon for the removal of micropollutants from municipal wastewater. *Science of The Total Environment*. 2019; *683*, 699-708.

46. KJ Howe, DW Hand, JC Crittenden, RR Trussell. Principles of water treatment. John Wiley & Sons; 2012.

47. Mazur, L. P., Pozdniakova, T. A., Mayer, D. A., Boaventura, R. A., & Vilar, V. J. Design of a fi xed-bed ion-exchange process for the treatment of rinse waters generated in the galvanization process using Laminaria hyperborea as natural cation exchanger. Water Research. 2016; 90:354–368.

48. Sing, K. S., & Williams, R. T. Physisorption hysteresis loops and the characterization of nanoporous materials. *Adsorption Science & Technology*. 2004; *22*(10), 773-782.

49. Moubarik, A., & Grimi, N. Valorization of olive stone and sugar cane bagasse by-products as biosorbents for the removal of cadmium from aqueous solution. Food Research International. 2015; 73, 169-175

50. Bhadra, B. N., Seo, P. W., & Jhung, S. H. Adsorption of diclofenac sodium from water using oxidized activated carbon. Chemical Engineering Journal. 2016; 301, 27-34.

51. Tan G, Yuan H, Liu Y, Xiao D. Removal of lead from aqueous solution with native and chemically modified corncobs. Journal of Hazardous Materials. 2010;174(1–3):740–745

52. Ozdemir, I., Şahin, M., Orhan, R., & Erdem, M. Preparation and characterization of activated carbon from grape stalk by zinc chloride activation. *Fuel processing technology*. 2014;*125*, 200-206

53. Yu, F., Sun, S., Han, S., Zheng, J., & Ma, J. Adsorption removal of ciprofloxacin by multi-walled carbon nanotubes with different oxygen contents from aqueous solutions. Chemical Engineering Journal. 2016; 285, 588-595

54. Yin, D., Xu, Z., Shi, J., Shen, L., & He, Z. Adsorption characteristics of ciprofloxacin on the schorl: kinetics, thermodynamics, effect of metal ion and mechanisms. Journal of Water Reuse and Desalination. 2017; 8(3), 350-359.

55. Huang, L., Wang, M., Shi, C., Huang, J., & Zhang, B. Adsorption of tetracycline and ciprofloxacin on activated carbon prepared from lignin with H3PO4 activation. *Desalination and Water Treatment*. 2014; *52*(13-15), 2678-2687.

56. Soldatkina, L., & Zavrichko, M. Equilibrium, kinetic, and thermodynamic studies of anionic dyes adsorption on corn stalks modified by cetylpyridinium bromide. *Colloids and Interfaces*. 2019; *3*(1), 4.

57. Pyrolysis A. Fourier transform infrared spectroscopic study of thermal degradation of sugar cane bagasse. 1996;2370(96).

58. Bilba, K., & Ouensanga, A. (1996). Fourier transform infrared spectroscopic study of thermal degradation of sugar cane bagasse. *Journal of Analytical and Applied Pyrolysis*, *38*(1-2), 61-73..

59. Essandoh, M., Kunwar, B., Pittman Jr, C. U., Mohan, D., & Mlsna, T. Sorptive removal of salicylic acid and ibuprofen from aqueous solutions using pine wood fast pyrolysis biochar. *Chemical Engineering Journal*. 2015; *265*, 219-227.

60. Peng, X., Hu, F., Huang, J., Wang, Y., Dai, H., & Liu, Z. Preparation of a graphitic ordered mesoporous carbon and its application in sorption of ciprofloxacin: kinetics, isotherm, adsorption mechanisms studies. *Microporous and Mesoporous Materials*. 2026; *228*, 196-206.

61. Li, X., Chen, S., Fan, X., Quan, X., Tan, F., Zhang, Y., & Gao, J. Adsorption of ciprofloxacin, bisphenol and 2-chlorophenol on electrospun carbon nanofibers: In comparison with powder activated carbon. *Journal of colloid and interface science*. 2015; *447*, 120-127.

62. Song, J. Y., Bhadra, B. N., & Jhung, S. H. Contribution of H-bond in adsorptive removal of pharmaceutical and personal care products from water using oxidized activated carbon. *Microporous and Mesoporous Materials*. 2017; *243*, 221-228.

63. Maddox, R. N. AL. H. Mass Transfer: fundamentals and Applications. Englewood-Cliffs, NJ: Prentice-Hall.; 1985.

64. Suriyanon, N., Punyapalakul, P., & Ngamcharussrivichai, C. Mechanistic study of diclofenac and carbamazepine adsorption on functionalized silica-based porous materials. *Chemical Engineering Journal*. 2013; *214*, 208-218.

65. Kumar, D., & Gaur, J. P. Chemical reaction-and particle diffusion-based kinetic modeling of metal biosorption by a Phormidium sp.-dominated cyanobacterial mat. *Bioresource Technology*. 2011; *102*(2), 633-640.

66. Thommes, M., Kaneko, K., Neimark, A. V., Olivier, J. P., Rodriguez-Reinoso, F., Rouquerol, J., & Sing, K. S. Physisorption of gases, with special reference to the evaluation of surface area and pore size distribution (IUPAC Technical Report). *Pure and Applied Chemistry*. 2015; *87*(9-10), 1051-1069.

67. Doğan, E. Investigation of ciprofloxacin removal from aqueous solution by nanofiltration process. 2016.

554 68. Zhang, C. L., Qiao, G. L., Zhao, F., & Wang, Y. Thermodynamic and kinetic parameters of
555 ciprofloxacin adsorption onto modified coal fly ash from aqueous solution. *Journal of Molecular*
556 *Liquids*. 2011; *163*(1), 53-56.

557 69. Wu, S., Li, Y., Zhao, X., Du, Q., Wang, Z., Xia, Y., & Xia, L. Biosorption behavior of ciprofloxacin
558 onto Enteromorpha prolifera: isotherm and kinetic studies. *International journal of*
559 *phytoremediation*. 2015; *17*(10), 957-961.

560 70. Worch, E. *Adsorption technology in water treatment: fundamentals, processes, and modeling*.
561 Walter de Gruyter. 2012.

562 71. Suresh, S., Srivastava, V. C., & Mishra, I. M. Isotherm, thermodynamics, desorption, and
563 disposal study for the adsorption of catechol and resorcinol onto granular activated
564 carbon. *Journal of Chemical & Engineering Data*. 2011; *56*(4), 811-818.

565 72. Khitous, M., Moussous, S., Selatnia, A., & Kherat, M. Biosorption of Cd (II) by Pleurotus mutilus
566 biomass in fixed-bed column: experimental and breakthrough curves analysis. *Desalination and*
567 *Water Treatment*. 2016; *57*(35), 16559-16570.

568 73. Nazari, G., Abolghasemi, H., Esmaieli, M., & Pouya, E. S. Aqueous phase adsorption of
569 cephalexin by walnut shell-based activated carbon: A fixed-bed column study. *Applied Surface*
570 *Science*. 2016; *375*, 144-153.

571 74. Han, R., Wang, Y., Zhao, X., Wang, Y., Xie, F., Cheng, J., & Tang, M. Adsorption of methylene
572 blue by phoenix tree leaf powder in a fixed-bed column: experiments and prediction of
573 breakthrough curves. *Desalination*. 2009; *245*(1-3), 284-297.

574

Table

Click here to download Table: Table 1-9.docx

Table 1. List of equilibrium and kinetic models.

	Model	Equation	Description	Reference
Equilibrium models	Langmuir	$\frac{C_e}{q_e} = \frac{C_e}{q_m} + \frac{1}{K_L q_m}$ $R_L = \frac{1}{1 + K_L C_o}$	(R_L = 0), favorable (0<R_L<1), linear (R_L = 1) or unfavorable (R_L>1)	(35,36)
	Freundlich	$\log q_e = \log K_F + \frac{1}{n} \log C_e$		(35)
	Brunauer-Emmet-Teller (BET)	$q_e = \frac{q_S C_{BET} C_e}{(C_s - C_e)\left[1 + (C_{BET} - 1)(\frac{C_e}{C_s})\right]}$		(37)
Kinetic models	Pseudo first order	$\log(q_e - q_t) = log q_e - k_1 t$		(38)
	Pseudo second order	$\frac{t}{q_t} = \frac{1}{K_2 q_e^2} + \frac{2}{q_e} t$		(39)
	Weber and Morris	$q_t = K_d t^{0.5} + C$ $R_i = 1 - \left(\frac{C}{q_{ref}}\right)$	R_i is the ratio of the initial adsorption amount (C) to the final adsorption amount (q_{ref})*	(40)

*q_{ref} (mg g^{-1}) is the solid phase concentration at time t = t_{ref} for an adsorption system; t_{ref} is the longest time in the adsorption process.

Table 2. Physical properties of SB and PAC.

Adsorbent	S_{BET} (m^2 g^{-1})	Internal surface area (m^2 g^{-1})	Single point desorption total pore volume of pores (cm^3 g^{-1})	Desorption average pore diameter (nm)
SB	2.55	--	0.0065	10.19
PAC	643.97	606.83	0.3569	2.21

Table 3. Chemical characteristics of SB and PAC.

Adsorbent	C	H	N	S	O	Moisture (%)	Ash (%)	Volatile matter (%)	Fixed carbon (%)	pH_{PZC}	Higher caloric value (Kcal/Kg)
SB	45.5	6.2	0.3	0.1	47.9	7.5	1.7	86.3	4.5	5.9	4102
PAC	85.8	1.2	0.2	0	12.8	10.3	1.6	2.3	85.8	7.6	6118

Table 4. Absorption bands of the functional groups in the untreated SB and PAC samples.

Functional groups	SB wave number (cm^{-1})	PAC wave number (cm^{-1})	Reference
O-H stretching	3338		(8,53,54)
C-H, stretching	2893	2940, 2485	(53,55)
C=O stretching	1726		(53,56)
C=C	1603	1578	(57)
skeletal modes	1513		(8,53)
C-H bending	1426		(8,53)
C–O stretching	1370		(57)
O-H Bending	1319		(57)
C-O-C, C-O	1239	1126	(57)
C-O-C, C-OH	1160	1056	(57)
O-H association	1034		(55,57)
C-H aromatic	900-600		(57,58)

Table 5. Kinetic parameters of CPX adsorption on SB and PAC.

Adsorbent	Experimental q_e ($mg\ g^{-1}$)	Pseudo-first order			Pseudo-second order			Weber and Morris	
		q_e ($mg\ g^{-1}$)	K_1 (min^{-1})	R^2	q_e ($mg\ g^{-1}$)	K_2 ($g\ mg^{-1}\ min^{-1}$)	R^2	C ($mg\ g^{-1}$)	R^2
SB	5.72	5.73	0.046	0.76	5.81	0.090	0.99	2.87	0.92
PAC	50.12	50.0	0.043	0.96	51.2	0.0045	0.99	27.31	0.91

Table 6. Langmuir, Freundlich and BET isotherm parameters of CPX adsorption onto SB and PAC.

Adsorbent	T (°C)	Langmuir				Freundlich			BET			
		q_m (mg g^{-1})	K_L (L mg^{-1})	R_L	R^2	K_F (mg L^{-1}) (mg $g^{-1})^{-1/n}$	n	R^2	C_s (mg L^{-1})	C_{BET} (L mg^{-1})	q_s (mg g^{-1})	R^2
SB	20	16.6	0.201	0.19	0.92	1.98	1.43	0.96	66.1	59.0	8.47	0.99
	30	13.69	0.139	0.23	0.93	1.28	1.56	0.98	70.0	49.62	6.99	0.98
	40	10.4	0.090	0.31	0.87	1.05	2.04	0.97	82.2	48.57	6.23	0.98
PAC	20	64.93	0.041	0.10	0.99	21.97	2.98	0.92	85	334.3	49.85	0.92
	30	71.94	0.059	0.08	0.99	34.15	3.06	0.87	79	121.1	45.89	0.89
	40	78.12	0.120	0.05	0.99	39.25	3.94	0.91	60	87.8	38.31	0.91

Table 7. Thermodynamic parameters of CPX adsorption on PAC and SB.

Adsorbent	T (°C)	ΔG° (KJ mol^{-1}	ΔH° (KJ mol^{-1})	ΔS° (J mol^{-1} K^{-1})	R^2
PAC	20	-23.14	41.31	0.21	0.98
	30	-24.84			
	40	-27.51			
SB	20	-26.99	-28.35	0.01	0.97
	30	-26.83			
	40	-26.56			

Table 8. Main results obtained in adsorption experiments in fixed bed columns (pH = 6, CPX = 10 mg L^{-1}, Q = 3 mL min^{-1}, bed density = 0.143 g cm^{-3}).

				C/Co = 0.1				C/Co = 0.9			
m (g)	H (cm)	H/d	t_b (min)	V_b (mL)	BV	BV*	q_b (mg g^{-1})	t_s (min)	q_s (mg g^{-1})	FBU %	MTZ (cm)
1.0	4	2.67	22	66	9.4	19.5	2.5	180	14.08	17.76	3.29
1.5	6	4.00	39	117	11.1	23.0	2.7	250	12.13	22.26	4.66
2.0	8	5.34	59	177	12.5	26.1	3.0	280	11.00	27.27	5.82
2.5	10	6.67	88	264	15.0	31.2	3.4	330	9.81	34.66	6.53
3.0	12	8.00	110	330	15.6	32.5	3.7	360	9.66	38.30	7.40
3.5	14	9.34	145	435	17.6	36.8	4.41	400	9.37	47.07	7.41

Legend: V_b volume of treated influent, d column diameter.

Table 9. Bohart-Adams parameters.

H (cm)	K_{BA} (L mg^{-1} min^{-1})	N_o (mg L^{-1})	R^2
4	0.0030	402.5	0.96
6	0.0028	366.5	0.98
8	0.0027	309.6	0.98
10	0.0026	293.9	0.97
12	0.0024	266.5	0.96
14	0.0023	265.2	0.94

Figure

Click here to download Figure: Figure 1.docx

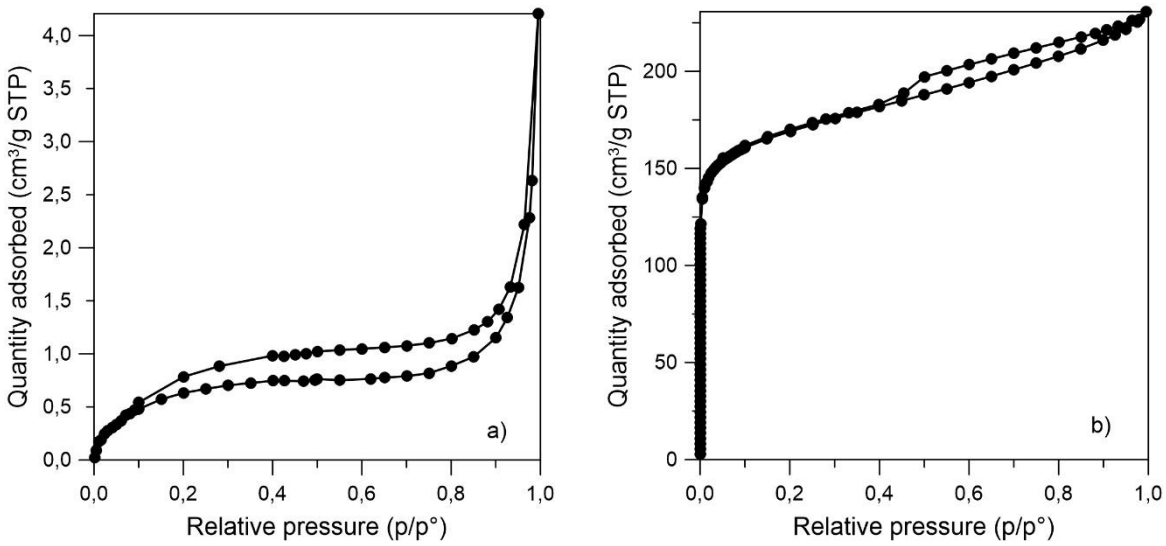

Figure 1. The adsorption/desorption isotherm of N_2 on SB a) and PAC b).

Figure

Click here to download Figure: Figure 2.docx

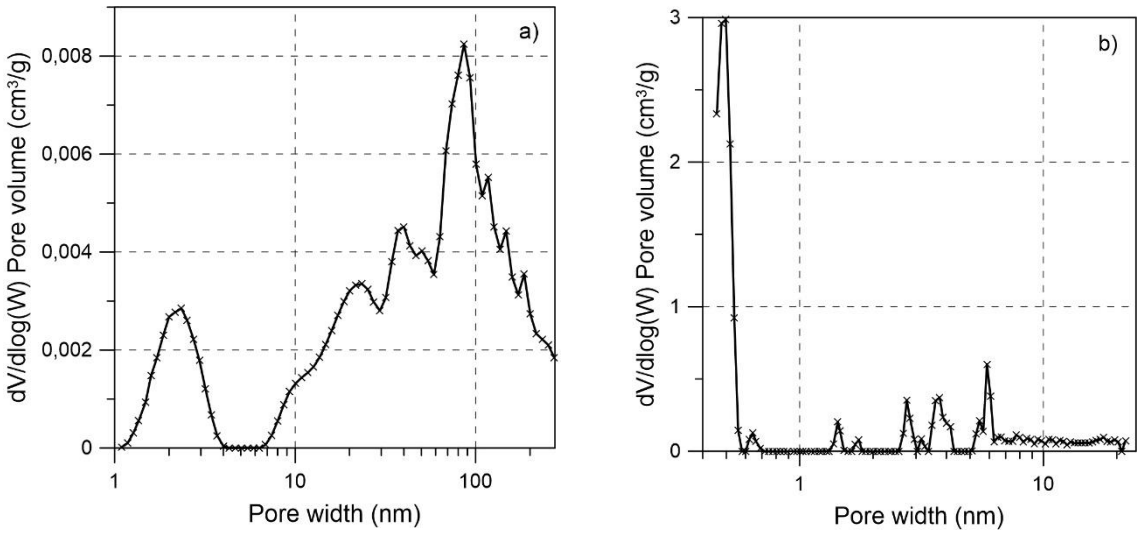

Figure 2. Pore size distribution of the SB a) and PAC b) sorbents.

Figure
Click here to download Figure: Figure 3.docx

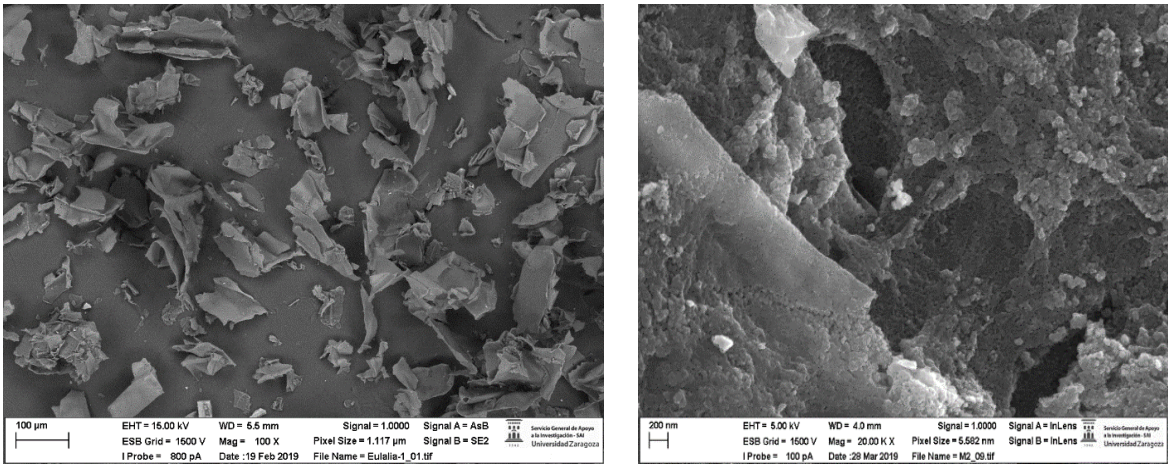

a) b)

Figure 3. SEM images of the surface of SB a) and PAC b).

Figure

Click here to download Figure: Figure 4.docx

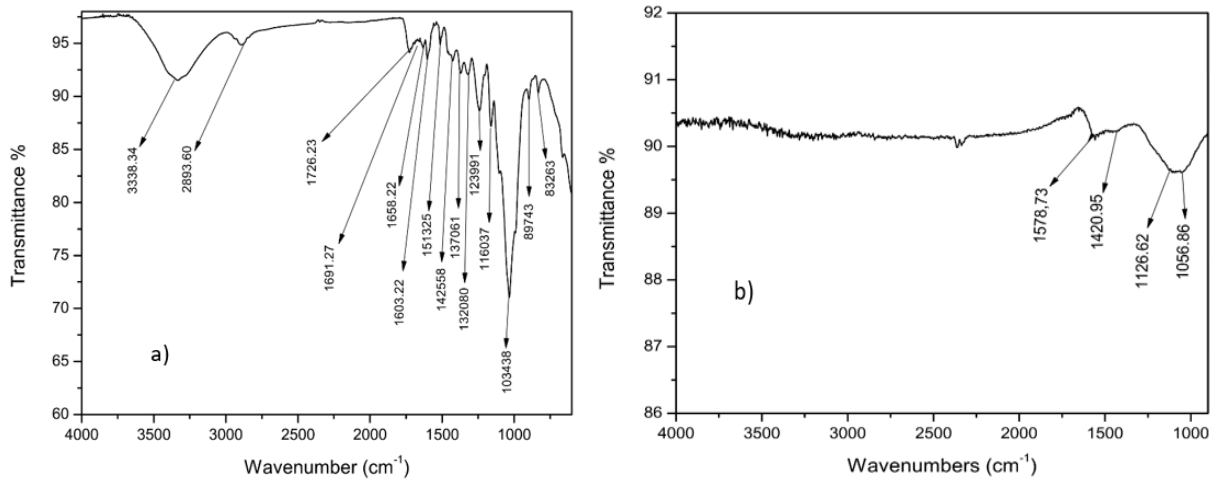

Figure 4. FTIR spectrum of SB a) and PAC b).

Figure

Click here to download Figure: Figure 5.docx

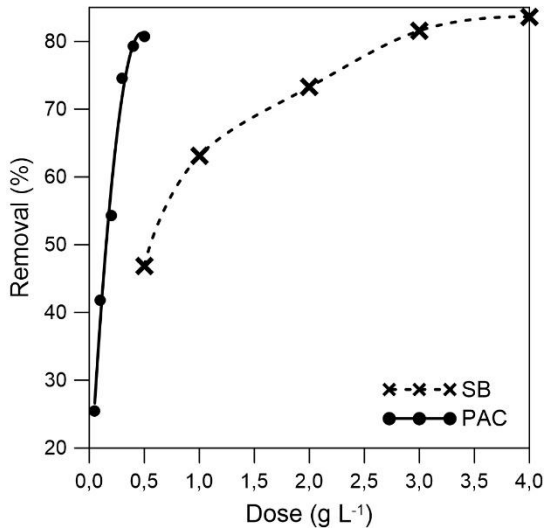

Figure 5. Influence of dosage on the adsorption capacity of CPX from aqueous solutions (pH 6, 30°C, 100 min, CPX: 20 mg L^{-1}).

Figure

Click here to download Figure: Figure 6.docx

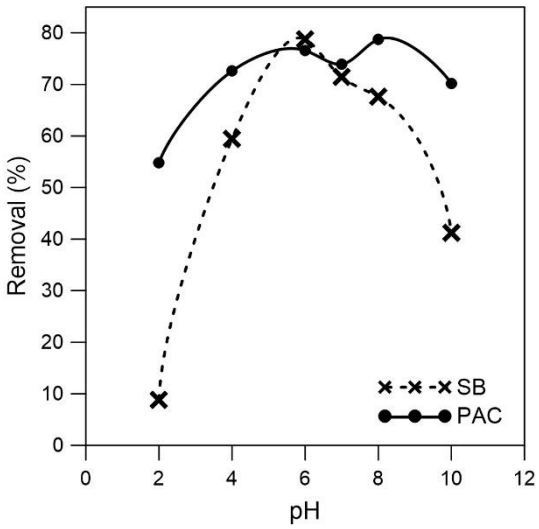

Figure 6. Influence of the pH on the adsorption of CPX on SB and PAC (CPX: 20 mg L^{-1}; PAC: 0.3 g L^{-1}; SB: 3 g L^{-1}).

Figure

Click here to download Figure: Figure 7.docx

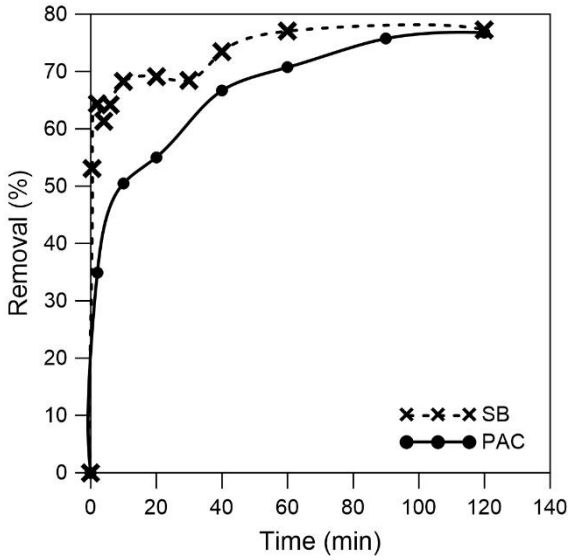

Figure 7. Percentage removal of CPX by SB and by PAC as a function of time (CPX: 20 mg L^{-1}, 30°C, PAC: 0.3 g L^{-1}; SB: 3 g L^{-1}, pH 6, 30 ºC).

Figure
Click here to download Figure: Figure 8.docx

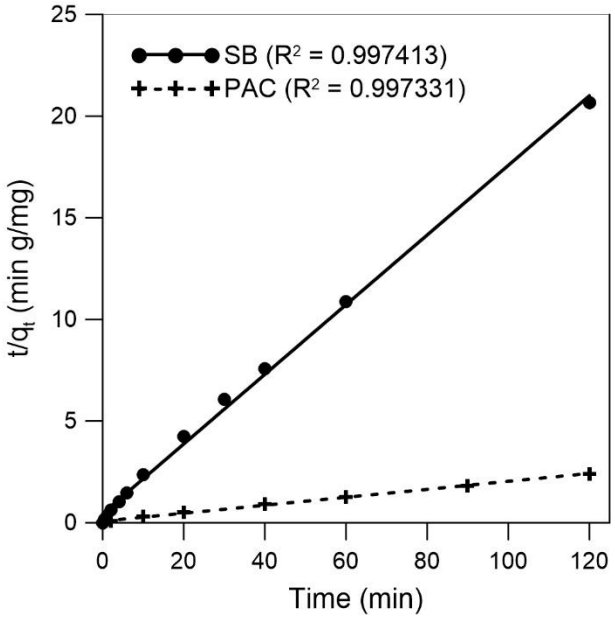

Figure 8. Pseudo-second-order kinetic plots for the adsorption of CPX on SB and PAC (CPX: 20 mg L^{-1}, 30°C, PAC: 0.3 g L^{-1}; SB: 3 g L^{-1}, pH 6, 30ºC).

Figure

Click here to download Figure: Figure 9.docx

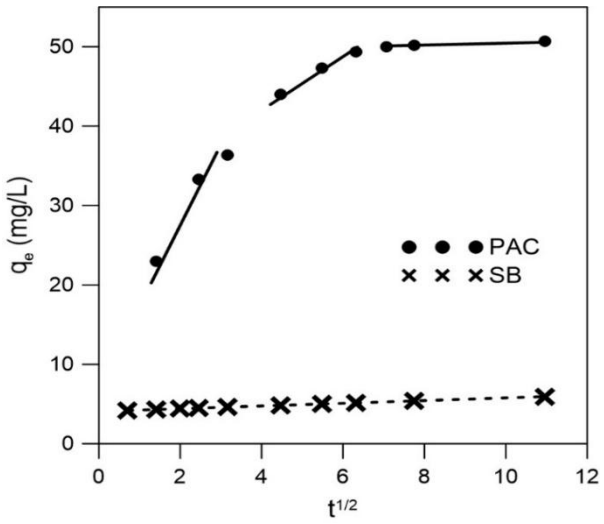

Figure 9. Plot of the intraparticle diffusion model of Weber and Morris for SB and PAC (CPX: 20 mg L^{-1}, PAC: 0.3 g L^{-1}; SB: 3 g L^{-1}, pH 6, 30°C).

Figure

Click here to download Figure: Figure 10.docx

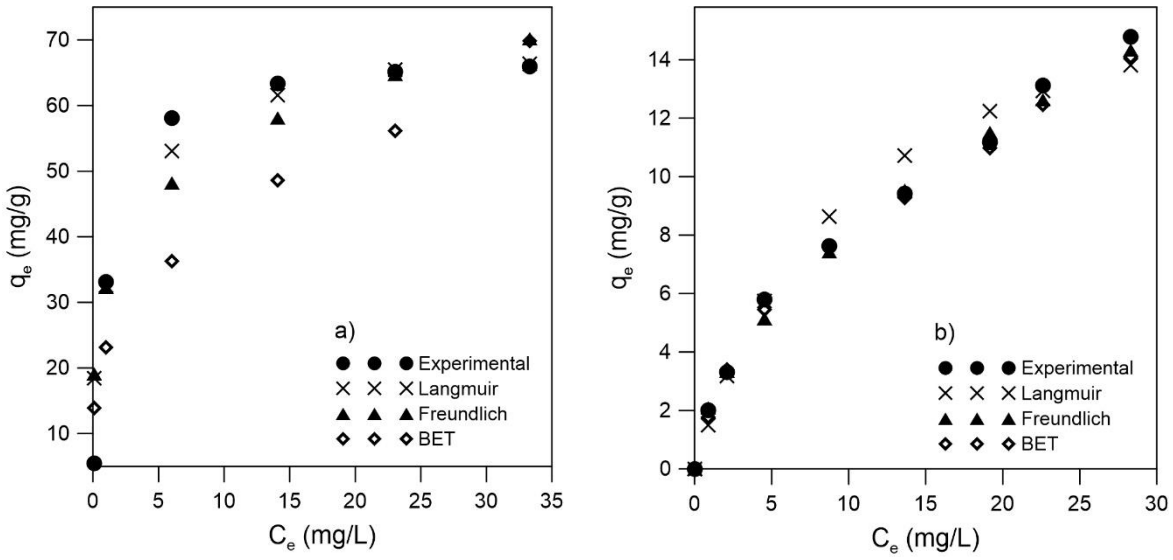

Figure 10. Adsorption isotherms of CPX on PAC a) and SB b) (CPX: 5 to 70 mg L^{-1}, PAC: 0.3 g L^{-1}; SB: 3 g L^{-1}, pH 6, 30°C, 120 min).

Figure

Click here to download Figure: Figure 11.docx

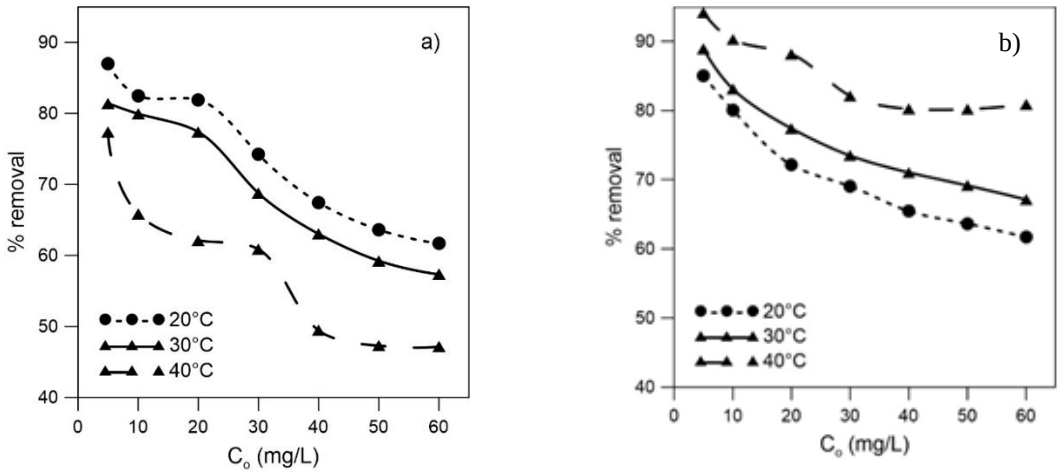

Figure 11. Effect of temperature on CPX adsorption: a) Variation of the % removal on SB; b) Variation of the % removal on PAC. (For isotherms of SB and PAC at different temperatures, see the Supplementary material Fig S1).

Figure

Click here to download Figure: Figure 12.docx

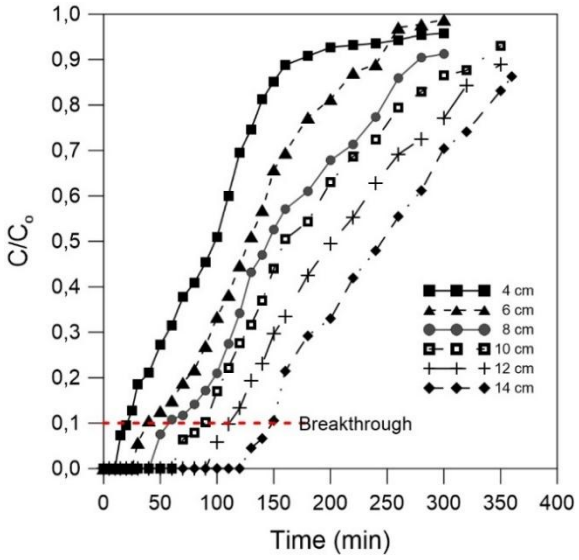

Figure 12. Curves of effluent concentration versus time for different bed heights (pH = 6, CPX: 10 mg L^{-1}, Q = 3 mL min^{-1}, bed density = 0.143 g cm^{-3}).

Figure

Click here to download Figure: Figure 13.docx

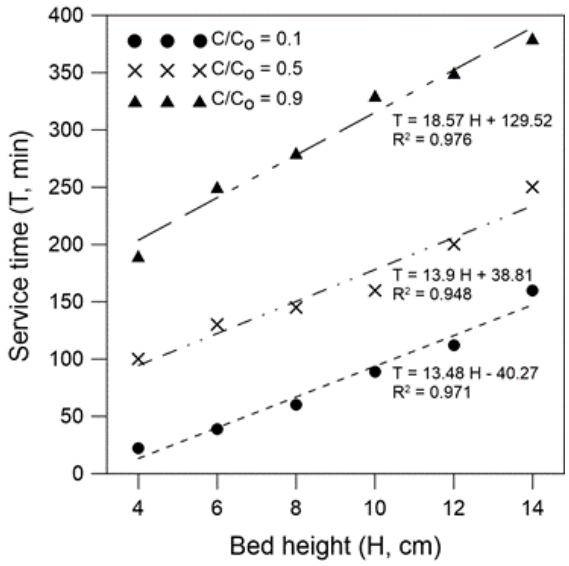

Figure 13. Relationship between bed height and service time.

Supplementary material for on-line publication only

Click here to download Supplementary material for on-line publication only: Supplementary material.docx

Credit Author Statement

Peñafiel: Methodology, Writing - Original Draft, Formal analysis, Investigation. **Matesanz.**: Formal analysis, Writing- Original draft preparation, Writing - Review & Editing. **Vanegas**: Visualization, Resources, Funding acquisition. **Bermejo***:* Investigation, Data curation, Software. **Mosteo**: Project administration. **Ormad**: Conceptualization, Supervision, Validation, Resources, Project administration.